Efficient Deep Red Light-Sensing All-Polymer Phototransistors with p-type/n-type Conjugated Polymer Bulk Heterojunction Layers

Sungho Nam[†,‡], *Jooyeok Seo*[†], *Hyemi Han*[†], *Hwajeong Kim*[†,§], *Donal D. C. Bradley*[‡,‖], *and Youngkyoo Kim**[,†]

[†]Organic Nanoelectronics Laboratory and KNU Institute for Nanophotonics Applications, Department of Chemical Engineering, School of Applied Chemical Engineering, Kyungpook National University, Daegu 41566, Republic of Korea

[‡]Department of Physics, Clarendon Laboratory, University of Oxford, Oxford OX1 3PU, United Kingdom.

[§]Priority Research Center, Research Institute of Advanced Energy Technology, Kyungpook National University, Daegu 41566, Republic of Korea.

[‖]Department of Engineering Science, Clarendon Laboratory, University of Oxford, Oxford OX1 3PJ, United Kingdom.

*Corresponding Author: Prof. Youngkyoo Kim
Email: ykimm@knu.ac.kr
Tel: +82-53-950-5616

ABSTRACT

Here we demonstrate deep red light-sensing all-polymer phototransistors with bulk heterojunction layers of poly[4,8-bis[(2-ethylhexyl)-oxy]benzo[1,2-b:4,5-b′]dithiophene-2,6-diyl][3-fluoro-2-[(2-ethylhexyl)carbonyl]thieno[3,4-b]-thiophenediyl] (PTB7) and poly[[N,N′-bis(2-octyldodecyl)-naphthalene-1,4,5,8-bis(dicarboximide)-2,6-diyl]-alt-5,5′-(2,2′-bithiophene)] (P(NDI2OD-T2)). The device performances were investigated by varying the incident light intensity of the deep red light (675 nm), while the signal amplification capability was examined by changing the gate and drain voltages. The result showed that the present all-polymer phototransistors exhibited higher photoresponsivity (~14 A/W) and better on/off photoswitching characteristics than the devices with the pristine polymers under illumination with the deep red light. The enhanced phototransistor performances were attributed to the well-aligned nanofiber-like morphology and nanocrystalline P(NDI2OD-T2) domains in the blend films, which are beneficial for charge separation and charge transport in the in-plane direction.

KEYWORDS: deep red light-sensing, all-polymer phototransistor, polymer/polymer bulk heterojunction layer, photoresponsivity, photoswitching

INTRODUCTION

Integrated optoelectronic sensors are designed to recognize patterns, images, motion, and colours by producing an electrical signal proportional to the light incident on their active areas.[1-5] Deep red light (650 – 700 nm) optical sensors have been widely used for biomedical and healthcare applications such as blood pressure, pulse oximetry, and muscle contraction sensing.[6-12] They must detect low-intensity transmitted and/or reflected light from tissues, muscles, and blood. Due to variation in optical signals from person to person, the development of a highly efficient deep red light-sensing device is important to provide more accurate readings and faster results.

Conjugated polymers have attractive properties such as tuneable light absorption, high optical density, biocompatibility, simplicity of fabrication on flexible substrates with scope for miniaturization, and mechanical robustness. The rational structural design of conjugated polymers with proper electronic energy levels and band gaps has resulted in significant breakthroughs.[13-16] Despite the successful development of novel materials, conjugated polymers suffer from the intrinsic limitation of high exciton binding energy (0.3 – 1 eV) because of their low dielectric constants ($\varepsilon \approx 2 - 4$).[17-19] However, the introduction of bulk heterojunction (BHJ) layers consisting of electron-donating (p-type) and electron-accepting (n-type) organic semiconductors with sufficient energy offsets can effectively separate tightly bound excitons.[20-21] Although BHJ layers have attracted considerable attention as light absorption layers for solar cells, we have focused on using BHJ layers in phototransistors, which can provide high gain by optically manipulating charge transport characteristics. In particular, all-polymer BHJ layers consisting of hole-transporting (p-type) and electron-transporting (n-type) polymers have great advantages such as morphological stability, mechanical flexibility, and thermal endurance, in

contrast to polymer:small molecule BHJ layers.[22-23] In addition, they can offer efficient charge separation and effective lateral charge transport. We have successfully demonstrated broadband light-sensing all-polymer phototransistors, which can detect near-infrared light up to 1000 nm, as well as ambipolar all-polymer phototransistors, which show outstanding light-sensing characteristics in both p-channel and n-channel modes of operation.[24-25] Although a systematic study of the solvent effect on the morphology, microstructure, and performance of PTB7:P(NDI2OD-T2) solar cells was examined in a previous report,[26-27] PTB7:P(NDI2OD-T2) BHJ layers have not yet been examined for phototransistor applications despite their outstanding optoelectronic properties.

In this paper, we fabricated all-polymer phototransistors with BHJ light-sensing layers that contained PTB7 electron-donating (*p*-type) and P(NDI2OD-T2) electron-accepting (*n*-type) polymers (see **Figure 1a**). We investigated the deep-red light photoresponse of all-polymer (PTB7:P(NDI2OD-T2) and P(NDI2OD-T2)-only phototransistors by varying the incident light intensities (P_{IN}) under 675 nm monochromatic light. The surface morphologies and nanostructures of pristine polymer and all-polymer BHJ layers were examined using atomic force microscopy (AFM), high resolution transmission electron microscopy (HRTEM), and synchrotron radiation grazing incidence angle X-ray diffraction (GIXD) measurements.

RESULTS AND DISCUSSION

All-polymer phototransistors composed of PTB7:P(NDI2OD-T2) light-sensing BHJ layers were fabricated in a top-gate/bottom-contact structure where the incident light is exposed only to the channel region in order to rule out changes in the contact resistance and reduce the exciton diffusion effect.[28-29] In a bilayer gate insulator, low-*k* PMMA (k = 3.5) can provide reduced

leakage current and charge trap density at interfaces between organic semiconductors and gate insulators, or in the bulk of the gate insulator, while high-*k* PVA (k = 7 − 8) can offer high capacitance.[25] **Figure 1b** presents the absorption spectra of pristine PTB7, P(NDI2OD-T2), and PTB7:P(NDI2OD-T2) BHJ layers. The PTB7:P(NDI2OD-T2) BHJ layers show broad absorption in the range of 500 to 850 nm. The pronounced shoulder peak at around 675 nm in blend films is critical for deep-red light sensing applications. As shown in **Figure 1c**, the highest occupied molecular orbital (HOMO) energy levels of the pristine PTB7 and P(NDI2OD-T2) thin films were confirmed −5.1 and −5.9 eV, respectively, via photoelectron yield spectroscopy (PEYS) measurements after calibration of the measured onset points as described in our previous reports.[30-31] The lowest unoccupied molecular orbital (LUMO) energy levels are −3.5 and −4.4 eV for PTB7 and P(NDI2OD-T2) polymers in the solid state, respectively, as calculated from the optical energy band gap and HOMO energy levels. As expected from the HOMO/LUMO energy offsets of the two polymers, the photoluminescence (PL) intensity decreases significantly with PTB7:P(NDI2OD-T2) nanolayers, providing evidence of charge separation in blend films.

Figure 1

First, we examined basic transistor characteristics in the dark. As seen in the output curves in **Figures 2a** and **S1,** PTB7:P(NDI2OD-T2) devices exhibit excellent n-type characteristics with distinguished linear and saturation regions. As shown in **Figure 2b**, the P(NDI2OD-T2)-only device shows good current modulation with electron mobility in saturation region (μ_e) of 1.1 $\times 10^{-1}$ $cm^2\ V^{-1}s^{-1}$, an I_{ON}/I_{OFF} ratio of 10^3 – 10^5, and a threshold voltage (V_{TH}) of 5.52 V. More importantly, all-polymer transistors based on PTB7:P(NDI2OD-T2) BHJ layers also exhibit

comparable electron transporting characteristics (μ_e = 1.02 ×10^{-1} cm^2 $V^{-1}s^{-1}$, I_{ON}/I_{OFF} ratio = 10^3 – 10^4, and V_{TH} = 5.91 V) despite the presence of 50 wt% of an electron-donating (p-type) PTB7 polymer in the blend films, resulting in slightly lower drain current (I_D) than for a pristine P(NDI2OD-T2) device. This indicates that PTB7:P(NDI2OD-T2) transistors exhibit minimal decreases in electron transport properties when compared to P(NDI2OD-T2)-only transistors. The blend films contain continuous P(NDI2OD-T2) domains in the lateral direction, but these do not significantly impede charge transport. In particular, both pristine P(NDI2OD-T2) and PTB7:P(NDI2OD-T2) transistors exhibit less gate voltage (V_G) dependent behaviour, which reflects that the equilibrium charge carrier concentration is in accordance with ideal current-voltage characteristics (see **Figure 2c**). Here, we note that there are no obvious ambipolar transport characteristics for the PTB7:P(NDI2OD-T2) transistors because of the poor hole transporting properties of PTB7 polymers (see **Figure S1**). This discrepancy between the ambipolar transport characteristics in this and previous report stem from the different device structures, solution concentrations, film thicknesses, and source-drain electrodes used.[27] In this work, we focus primarily on studying the electron-transport characteristics of pristine P(NDI2OD-T2) and PTB7:P(NDI2OD-T2) phototransistors.

Figure 2

We investigated the characteristics of pristine P(NDI2OD-T2) and PTB7:P(NDI2OD-T2) phototransistors under 675 nm light as a function of incident light intensity (P_{IN}). The 675 nm wavelength was chosen because of its strong absorption by pristine P(NDI2OD-T2) and PTB7:P(NDI2OD-T2) blend films. As shown in the output and transfer curves of **Figures 3a**

and 3b, I_D increases for pristine P(NDI2OD-T2)-only and PTB7:P(NDI2OD-T2) devices as P_{IN} increases, which indicates that P_{IN} can play an important role in modulating charge carriers in the light-sensing layer. In particular, we found that the I_D increment at V_D and V_G = 40 V was ca. 8 times higher for PTB7:P(NDI2OD-T2) devices than for a P(NDI2OD-T2)-only device (ΔI_D = 140 nA at 23 μW/cm^2 and ΔI_D = 900 nA at 21 μW/cm^2 for P(NDI2OD-T2) and PTB7:P(NDI2OD-T2) phototransistors, respectively) (see **Figure 3c**). This observation supports the hypothesis that the photogenerated charges (excitons) in the pristine P(NDI2OD-T2) polymer do not separate into holes and electrons due to their strong exciton binding energies. However, the photogenerated charges (excitons) in blend films can be efficiently dissociated at the interfaces between PTB7 and P(NDI2OD-T2) domains and transported within P(NDI2OD-T2) domains. Note that the relatively low I_{DP}/I_{DD} ratio can be attributed to the PMMA gate insulator characteristics. There is less change in the contact resistance because only the channel region is under illumination. In particular, we found that the V_{TH} shifts towards a negative bias for both devices (see **Figure S4**) because of photogenerated holes trapped at the interfaces between the polymers and the gate insulators. As shown in **Figure 3d**, the V_{TH} shift (ΔV_{TH}) is proportional to P_{IN} regardless of the device type. In particular, ΔV_{TH} was higher for the PTB7:P(NDI2OD-T2) device than for the P(NDI2OD-T2)-only device, suggesting that more photogenerated holes were trapped at the interface between the BHJ layers and the gate insulators. In addition, we calculated the trapped hole surface density (ΔN_i) using the following equation: $\Delta N_i = (\Delta V_{TH} \times C_i) / q$, where N_i, C_i, and q are the trapped hole surface density, the capacitance of the gate insulator, and the elementary charge, respectively.[32-33] This reveals that more photogenerated holes are trapped with the PTB7:P(NDI2OD-T2) phototransistor ($\Delta N_i = 3.14 \times 10^{10}$ at 21 μW/cm^2) than with the P(NDI2OD-T2)-only device ($\Delta N_i = 1.94 \times 10^{10}$ at 23 μW/cm^2). This result suggests that charge

transferred holes from the PTB7 polymer as well as photogenerated holes in the P(NDI2OD-T2) polymer are trapped at the interface, and thus the overall electron carrier density in the channel region increases, leading to high I_D for PTB7:P(NDI2OD-T2) phototransistors.

Figure 3

We investigated the photoresponsivity (R_C) in order to evaluate device performance. The photoresponsivity can be calculated using the following equation: $R_C = (I_{DP} - I_{DD})/(P_{IN} \times A)$ where I_{DP}, I_{DD}, and A are the drain current in light, the drain current in the dark, and the active illuminated area, respectively.[34-35] As shown in **Figures 4a** and **S5**, the R_C values gradually increase with the drain voltage (V_D) for both devices, and higher R_C values are shown when the devices are exposed at lower P_{IN}. The decrease in R_C as P_{IN} increases can be explained by the high charge recombination rate. A similar increase in R_C was measured as a function of gate voltage (V_G) (see **Figures 4c** and **S6**), confirming that our all-polymer phototransistors are sensitive to monochromatic light at 675 nm. The highest R_C value for PTB7:P(NDI2OD-T2) phototransistors at V_D and V_G = 40 V, and P_{IN} = 21 μW/cm^2 was 14.2 A/W, which is ca. 4 – 6 times higher than with a pristine P(NDI2OD-T2) device (2.3 A/W from output curves and 3.2 A/W from transfer curves at V_D and V_G = 40 V, and P_{IN} = 23 μW/cm^2). In addition, the trend of P_{IN}-dependent R_C here is in accordance with those in our previous reports.[25,36] R_C can be expressed simply using a power law relationship ($R_C \sim P_{IN}^{\alpha}$). The R_C values of PTB7:P(NDI2OD-T2) phototransistors are more P_{IN}-dependent than those of P(NDI2OD-T2)-only devices (see **Figure 4b**). In addition, the R_C values of PTB7:P(NDI2OD-T2)

phototransistors are the more gate-voltage dependent than those of P(NDI2OD-T2)-only devices. This indicates more effective signal amplification via gate voltage control (see **Figure 4d**).

Figure 4

We sought insight into the photoresponse of P(NDI2OD-T2)-only and PTB7:P(NDI2OD-T2) phototransistors under pulse illumination at 675 nm and 1 Hz (see **Figure 5a**). As shown in **Figure 5b**, the P(NDI2OD-T2) device exhibits no photoresponse despite the relatively high P_{IN} (1550 μW/cm^2). However, excellent photoswitching and reversible behaviour, originating from the photogenerated electrons, was observed in PTB7:P(NDI2OD-T2) phototransistors even at the lowest P_{IN} of 21 μW/cm^2 (see **Figure 5c**). This result suggests that electron-hole recombination is dominant within the illumination time of P(NDI2OD-T2)-only devices, while the excitons (hole-electron pairs) can be photo-generated by 675 nm monochromatic light in PTB7 and P(NDI2OD-T2) polymers. These excitons can be separated at the interfaces between PTB7 and P(NDI2OD-T2) via hole transfer from P(NDI2OD-T2) to PTB7 and electron transfer from PTB7 and P(NDI2OD-T2), respectively. The photogenerated electrons can be transported in P(NDI2OD-T2) domains and contribute to the photocurrent in all-polymer phototransistors (see **Figure S7**). Thus, PTB7:P(NDI2OD-T2) phototransistors show better photoresponses than pristine P(NDI2OD-T2) phototransistors due to fast charge separation at the interfaces between the PTB7 and P(NDI2OD-T2) polymer domains.

Figure 5

We investigated the surface morphologies of the pristine PTB7, P(NDI2OD-T2), and PTB7:P(NDI2OD-T2) BHJ layers via atomic force microscopy (AFM). As shown in **Figure 6a**, the AFM image of a pristine PTB7 thin film reveals a smooth, uniform surface with a relatively low root-mean square roughness (R_{RMS} = 0.35 nm), whereas the pristine P(NDI2OD-T2) film shows a relatively large, aggregated, nanofiber-like surface morphology with a rough surface (R_{RMS}= 0.72 nm). More importantly, the PTB7:P(NDI2OD-T2) BHJ layers exhibit relatively fine nanofiber-like morphologies with moderate roughness (R_{RMS}= 0.41 nm). Transmission electron microscopy (TEM) images of the pristine PTB7, P(NDI2OD-T2), and PTB7:P(NDI2OD-T2) BHJ layers further support this surface morphology analysis. As can be seen in **Figure 6b**, typical amorphous features of pristine PTB7 polymer are observed, whereas the pristine P(NDI2OD-T2) polymer exhibits a relatively large nanofiber-like morphology with highly crystalline features, as shown in the AFM images. In particular, the well-aligned, nanofiber-like structure in the TEM images of PTB7:P(NDI2OD-T2) BHJ layers is in line with the AFM images. In addition, scanning TEM (STEM) images of PTB7:P(NDI2OD-T2) BHJ layers provide direct observation of relatively fine nanophase separation between two polymer domains (see **Figure S8**). Hence, the improved device performance with PTB7:P(NDI2OD-T2) phototransistors may be closely related to the fine, well-connected nanofiber-like domains and interpenetrated nanophase separation in blend films. This morphology may provide sufficient interfacial area for charge separation and facilitate charge transport in the lateral direction.

Figure 6

In addition to surface morphology and nanostructure analysis, we performed synchrotron radiation grazing incidence angle X-ray diffraction (GIXD) measurements. As shown in the 2D GIXD images (see **Figures 7a** and **S9**), distinct face-on chain ordering is observed for both pristine PTB7 and P(NDI2OD-T2) thin films based on the previously reported predominant (100) peak in the IP direction and the (010) peak in OOP direction.[26,37] The PTB7 polymer exhibits a relatively amorphous structure, while the P(NDI2OD-T2) polymer has a highly ordered crystalline structure. As shown in **Figure 7b**, the PTB7:P(NDI2OD-T2) BHJ layer exhibits less intense but distinctive (100) and (001) peaks corresponding to crystalline P(NDI2OD-T2) nanodomains. These peaks were found in the blend films as well, which indicates that PTB7 and P(NDI2OD-T2) are phase-segregated, as evidenced by the AFM and TEM images. In addition, we calculated the P(NDI2OD-T2) crystallite size in pristine and blend films using the Scherrer equation.[38] Crystallite sizes of 6.45 and 4.78 nm were calculated for pristine P(NDI2OD-T2) and PTB7:P(NDI2OD-T2) films, respectively. This result suggests that relatively small P(NDI2OD-T2) crystallites are present in the BHJ layer. This is in line with the AFM and TEM images. Therefore, the combination of favourable nanophase separation between the relatively amorphous PTB7 polymer and the crystalline P(NDI2OD-T2) polymer, and relatively small crystallites can contribute to charge separation and transport in PTB7:P(NDI2OD-T2) phototransistors.

Figure 7

CONCLUSIONS

In summary, all-polymer phototransistors were fabricated using the BHJ layers that consist of PTB7 and P(NDI2OD-T2) polymers. As evidenced by PL quenching, the proper HOMO/LUMO energy offsets of the two polymers provided the driving force for charge separation. This indicates that they might be promising candidates for use in phototransistors. The electron-dominant transport in the PTB7:P(NDI2OD-T2) blend films suggests that the P(NDI2OD-T2) domains could be well-connected in the in-plane direction without charge blocking resistance, despite the presence of PTB7 polymers in the blend films. All-polymer phototransistors exhibited gradually increased photocurrent with the incident light intensity of the deep red light (675 nm). In contrast, the P(NDI2OD-T2)-only device showed lower sensitivity because of inherent limitations related to charge separation. The maximum R_C for all-polymer phototransistors could be as high as 14 A/W, whereas the pristine P(NDI2OD-T2) device reached only 2.3 ~ 3.2 A/W. The present all-polymer phototransistors showed fast photoswitching responses under light on/off modulation, which was assigned to the fast charge transport in the in-plane direction due to the well-aligned nanofiber-like morphology and smaller P(NDI2OD-T2) nanocrystallites in the blend films. Hence the present study is expected to contribute to further development of all-polymer phototransistors for deep red light-sensing devices which are of crucial importance in the coming ubiquitous healthcare monitoring systems.

METHODS

Materials and Solutions. PTB7 (weight-average molecular weight = 92 kDa, PDI = 2.6) and P(NDI2OD-T2) (weight-average molecular weight = 25 − 50 kDa, polydispersity index (PDI) = 1.5 − 3.5) were purchased from 1-Material (Canada) and Polyera (United States), respectively. PMMA (weight-average molecular weight = 120 kDa, PDI = 2.2) and PVA (weight-average

molecular weight = 13 – 23 (18) kDa, 98% hydrolysed) were purchased from Sigma-Aldrich (United States). The pristine polymer (PTB7 and P(NDI2OD-T2)) and blend (PTB7:P(NDI2OD-T2) = 5:5 by weight) solutions were prepared in chlorobenzene at a solid concentration of 10 mg/ml. The solutions of PMMA and PVA polymers were prepared using n-butyl acetate and deionized water at a solid concentration of 40 mg/ml and 80 mg/ml, respectively. All solutions prepared were vigorously stirred on a magnetic stirring plate for 24 h before spin-coating.

Thin Film and Device Fabrication. Glass substrates were cleaned via ultrasonication in acetone and isopropyl alcohol, then dried with nitrogen gas flows. 60 nm-thick silver (Ag) source/drain electrodes were deposited onto the glass substrates through a shadow mask at a base pressure of 2×10^{-6} Torr. The channel width and length were 2 mm and 70 μm, respectively. The pristine (PTB7 and P(NDI2OD-T2)) polymer and binary blend layers were spin-coated on the glass substrates. The thickness of all the photo-active layers was adjusted to 30 nm. Next, 350 nm-thick PMMA layers were spin-coated on the photo-active layers, followed by soft-baking at 60 ^{o}C for 30 min. Then 150 nm-thick PVA layers were spin-coated on the PMMA layers and soft-baked at 60 ^{o}C for 3 h. The capacitance of the PMMA/PVA bilayer gate insulators was 7.4 nF/cm^2 at 100 Hz. After transferring the samples to a vacuum chamber, 80 nm-thick aluminium (Al) was thermally evaporated on top of the PVA layers.

Device Measurements. The film thickness was measured using a surface profiler (Alpha Step 20, Tencor Instruments). The optical absorption and PL spectra were measured using a UV-visible spectrometer (Optizen 2120, MECASYS) and a PL spectrometer (FS-2, SCINCO), respectively. The HOMO energy levels of the pristine films were measured using a photoelectron yield spectrometer (AC2, Riken-Keiki), while the capacitance of the bilayer-type gate insulators were measured using an impedance analyser (VERSA STAT 4, Ametek, Berwyn, PA). An

atomic force microscope (AFM, Nanoscope V multimode 8, Bruker) was used to measure the surface morphology of films. Crystalline structures were measured using a field-emission/scanning transmission electron microscope (FE-TEM/STEM, Titan G2 ChemiSTEM Cs Probe, FEI Company) and a synchrotron radiation-grazing incidence X-ray diffraction (GIXD) system (X-ray wavelength = 0.11352 nm, incidence angle = 0.12 º, 9 A, U-SAXS beamline, Pohang Accelerator Laboratory). The transistor characteristics of devices were measured using a semiconductor parameter analyser (2636B, Keithley) and a specialized phototransistor measurement system equipped with a light source (Tungsten-Halogen lamp, 150 W, ASBN-W, Spectral Products) and monochromator (CM110, Spectra Products). The incident light intensity (P_{IN}) was measured using a calibrated Si photodiode (818-UV, Newport).

ACKNOWLEDGMENTS

This work was financially supported by grants from the Korean Government (NRF_2015R1A2A2A01003743, NRF_2014R1A1A3051165, NRF_2016H1D5A1910319, Human Resource Training Project for Regional Innovation_MOE_NRF-2014H1C1A1066748, and Basic Science Research Program_2009-0093819). We thank Prof. Christopher R. McNeill (Monash University) for his valuable contribution including polymer materials.

Supporting Information Available: Output and transfer curves of devices in the dark and under illumination, photoresponsitivity as a function of V_D and V_G at different P_{IN} levels, device mechanisms, STEM images, and enlarged 2D GIXD images are available via the Internet at http://pubs.acs.org.

REFERENCES

(1) Baeg, K. J.; Binda, M.; Natali, D.; Caironi, M.; Noh, Y. Y. Organic Light Detectors: Photodiodes and Phototransistors. *Adv. Mater.* **2013,** *25*, 4267-4295.

(2) Dong, H.; Zhu, H.; Meng, Q.; Gong, X.; Hu, W. Organic Photoresponse Materials and Devices. *Chem. Soc. Rev.* **2012,** *41*, 1754-808.

(3) Gu, P.; Yao, Y.; Feng, L.; Niu, S.; Dong, H. Recent Advances in Polymer Phototransistors. *Polym. Chem.* **2015,** *6*, 7933-7944.

(4) Guo, Y.; Yu, G.; Liu, Y. Functional Organic Field-Effect Transistors. *Adv. Mater.* **2010,** *22*, 4427-4447.

(5) Lucas, B.; Trigaud, T.; Videlot-Ackermann, C. Organic Transistors and Phototransistors Based on Small Molecules. *Polym. Int.* **2012,** *61*, 374-389.

(6) Gasser, C.; Taiber, S.; Yeh, C. M.; Wittig, C. H.; Hegemann, P.; Ryu, S.; Wunder, F.; Moglich, A. Engineering of a Red-Light-Activated Human Camp/Cgmp-Specific Phosphodiesterase. *Proc. Natl. Acad. Sci. U. S. A.* **2014,** *111*, 8803-8808.

(7) Kang, D.; Gai, B.; Thompson, B.; Lee, S.-M.; Malmstadt, N.; Yoon, J. Flexible Opto-Fluidic Fluorescence Sensors Based on Heterogeneously Integrated Micro-Vcsels and Silicon Photodiodes. *ACS Photon.* **2016,** *3*, 912-918.

(8) Karpenko, I. A.; Collot, M.; Richert, L.; Valencia, C.; Villa, P.; Mely, Y.; Hibert, M.; Bonnet, D.; Klymchenko, A. S. Fluorogenic Squaraine Dimers with Polarity-Sensitive Folding as Bright Far-Red Probes for Background-Free Bioimaging. *J. Am. Chem. Soc.* **2015,** *137*, 405-12.

(9) Li, Y.; Wang, Y.; Yang, S.; Zhao, Y.; Yuan, L.; Zheng, J.; Yang, R. Hemicyanine-Based High Resolution Ratiometric Near-Infrared Fluorescent Probe for Monitoring Ph Changes in Vivo. *Anal. Chem.* **2015,** *87*, 2495-503.

(10) Ni, Y.; Wu, J. Far-Red and near Infrared Bodipy Dyes: Synthesis and Applications for Fluorescent pH Probes and Bio-Imaging. *Org. Biomol. Chem.* **2014,** *12*, 3774-3791.

(11) Tahirbegi, I. B.; Ehgartner, J.; Sulzer, P.; Zieger, S.; Kasjanow, A.; Paradiso, M.; Strobl, M.; Bouwes, D.; Mayr, T. Fast Pesticide Detection inside Microfluidic Device with Integrated Optical Ph, Oxygen Sensors and Algal Fluorescence. *Biosens. Bioelectron.* **2016**, *88*, 188-195.

(12) Yoshihara, T.; Hosaka, M.; Terata, M.; Ichikawa, K.; Murayama, S.; Tanaka, A.; Mori, M.; Itabashi, H.; Takeuchi, T.; Tobita, S. Intracellular and in Vivo Oxygen Sensing Using Phosphorescent Ir(III) Complexes with a Modified Acetylacetonato Ligand. *Anal. Chem.* **2015,** *87*, 2710-2717.

(13) Zhao, Y.; Guo, Y.; Liu, Y. 25th Anniversary Article: Recent Advances in N-Type and Ambipolar Organic Field-Effect Transistors. *Adv. Mater.* **2013,** *25*, 5372-5391.

(14) Wang, Y.; Michinobu, T. Benzothiadiazole and Its Π-Extended, Heteroannulated Derivatives: Useful Acceptor Building Blocks for High-Performance Donor–Acceptor Polymers in Organic Electronics. *J. Mater. Chem. C* **2016,** *4*, 6200-6214.

(15) Wang, C.; Dong, H.; Hu, W.; Liu, Y.; Zhu, D. Semiconducting Pi-Conjugated Systems in Field-Effect Transistors: A Material Odyssey of Organic Electronics. *Chem. Rev.* **2012,** *112*, 2208-2267.

(16) Holliday, S.; Donaghey, J. E.; McCulloch, I. Advances in Charge Carrier Mobilities of Semiconducting Polymers Used in Organic Transistors. *Chem. Mater.* **2014,** *26*, 647-663.

(17) Beaujuge, P. M.; Frechet, J. M. Molecular Design and Ordering Effects in Pi-Functional Materials for Transistor and Solar Cell Applications. *J. Am. Chem. Soc.* **2011,** *133*, 20009-20029.

(18) Boudreault, P.-L. T.; Najari, A.; Leclerc, M. Processable Low-Bandgap Polymers for Photovoltaic Applications. *Chem. Mater.* **2011,** *23*, 456-469.

(19) Zhou, H.; Yang, L.; You, W. Rational Design of High Performance Conjugated Polymers for Organic Solar Cells. *Macromolecules* **2012,** *45*, 607-632.

(20) Dang, M. T.; Hirsch, L.; Wantz, G.; Wuest, J. D. Controlling the Morphology and Performance of Bulk Heterojunctions in Solar Cells. Lessons Learned from the Benchmark Poly(3-Hexylthiophene):[6,6]-Phenyl-C61-Butyric Acid Methyl Ester System. *Chem. Rev.* **2013,** *113*, 3734-3765.

(21) Heeger, A. J. 25th Anniversary Article: Bulk Heterojunction Solar Cells: Understanding the Mechanism of Operation. *Adv. Mater.* **2014,** *26*, 10-27.

(22) Kim, T.; Kim, J. H.; Kang, T. E.; Lee, C.; Kang, H.; Shin, M.; Wang, C.; Ma, B.; Jeong, U.; Kim, T. S.; Kim, B. J. Flexible, Highly Efficient All-Polymer Solar Cells. *Nat. Commun.* **2015,** *6*, 8547.

(23) Facchetti, A. Polymer Donor–Polymer Acceptor (All-Polymer) Solar Cells. *Mater. Today* **2013,** *16*, 123-132.

(24) Han, H.; Nam, S.; Seo, J.; Lee, C.; Kim, H.; Bradley, D. D.; Ha, C. S.; Kim, Y. Broadband All-Polymer Phototransistors with Nanostructured Bulk Heterojunction Layers of Nir-Sensing N-Type and Visible Light-Sensing P-Type Polymers. *Sci. Rep.* **2015,** *5*, 16457.

(25) Nam, S.; Han, H.; Seo, J.; Kim, H.; Anthopoulos, T. D.; McCulloch, I.; Bradley, D. D. C.; Kim, Y. Ambipolar Organic Phototransistors with P-Type/N-Type Conjugated Polymer Bulk Heterojunction Light-Sensing Layers. *Adv. Electron. Mater.* **2016**, *2*, 1600264.

(26) Tang, Y.; McNeill, C. R. All-Polymer Solar Cells Utilizing Low Band Gap Polymers as Donor and Acceptor. *J. Polym. Sci., Part B: Polym. Phys.* **2013,** *51*, 403-409.

(27) Zhou, N.; Lin, H.; Lou, S. J.; Yu, X.; Guo, P.; Manley, E. F.; Loser, S.; Hartnett, P.; Huang, H.; Wasielewski, M. R.; Chen, L. X.; Chang, R. P. H.; Facchetti, A.; Marks, T. J. Morphology-Performance Relationships in High-Efficiency All-Polymer Solar Cells. *Adv. Energy Mater.* **2014,** *4*, 1300785.

(28) Singh, T. B.; Koeppe, R.; Sariciftci, N. S.; Morana, M.; Brabec, C. J. Monitoring the Channel Formation in Organic Field-Effect Transistors Via Photoinduced Charge Transfer. *Adv. Funct. Mater.* **2009,** *19*, 789-795.

(29) Narayan, K. S.; Kumar, N. Light Responsive Polymer Field-Effect Transistor. *Appl. Phys. Lett.* **2001,** *79*, 1891-1893.

(30) Nam, S.; Shin, M.; Kim, H.; Ha, C.-S.; Ree, M.; Kim, Y. Improved Performance of Polymer:Polymer Solar Cells by Doping Electron-Accepting Polymers with an Organosulfonic Acid. *Adv. Funct. Mater.* **2011,** *21*, 4527-4534.

(31) Kim, H.; Shin, M.; Kim, Y. Long Time Thermal Annealing Effects on the Film Morphology and Performance of Polymer Solar Cells with Calcium Electrode. *Macromol. Res.* **2009,** *17*, 445-447.

(32) Milvich, J.; Zaki, T.; Aghamohammadi, M.; Rödel, R.; Kraft, U.; Klauk, H.; Burghartz, J. N. Flexible Low-Voltage Organic Phototransistors Based on Air-Stable Dinaphtho[2,3-B:2′,3′-F]Thieno[3,2-B]Thiophene (DNTT). *Org. Electron.* **2015,** *20*, 63-68.

(33) Miscioscia, R.; Loffredo, F.; Nenna, G.; Villani, F.; Minarini, C.; Petrosino, M.; Rubino, A.; Denti, M.; Facchetti, A. Analysis of the Persistent Photoresponse of C8BTBT Transistors in the Near-Bandgap Spectral Region. *Org. Electron.* **2016,** *30*, 83-91.

(34) El Gemayel, M.; Treier, M.; Musumeci, C.; Li, C.; Mullen, K.; Samori, P. Tuning the Photoresponse in Organic Field-Effect Transistors. *J. Am. Chem. Soc.* **2012,** *134*, 2429-2433.

(35) Labram, J. G.; Wöbkenberg, P. H.; Bradley, D. D. C.; Anthopoulos, T. D. Low-Voltage Ambipolar Phototransistors Based on a Pentacene/PC61BM Heterostructure and a Self-Assembled Nano-Dielectric. *Org. Electron.* **2010,** *11*, 1250-1254.

(36) Han, H.; Nam, S.; Seo, J.; Jeong, J.; Kim, H.; Bradley, D. D. C.; Kim, Y. Organic Phototransistors with All-Polymer Bulk Heterojunction Layers of p-Type and n-Type Sulfur-Containing Conjugated Polymers. *IEEE J. Sel. Top. Quantum Electron.* **2016**, *22*, 6000107.

(37) Nam, S.; Woo, S.; Seo, J.; Kim, W. H.; Kim, H.; McNeill, C. R.; Shin, T. J.; Bradley, D. D.; Kim, Y. Pronounced Cosolvent Effects in Polymer:Polymer Bulk Heterojunction Solar Cells with Sulfur-Rich Electron-Donating and Imide-Containing Electron-Accepting Polymers. *ACS Appl. Mater. Interfaces* **2015,** *7*, 15995-16002.

(38) Shin, M.; Kim, H.; Park, J.; Nam, S.; Heo, K.; Ree, M.; Ha, C.-S.; Kim, Y. Abrupt Morphology Change Upon Thermal Annealing in Poly(3-Hexylthiophene)/Soluble Fullerene Blend Films for Polymer Solar Cells. *Adv. Funct. Mater.* **2010,** *20*, 748-754.

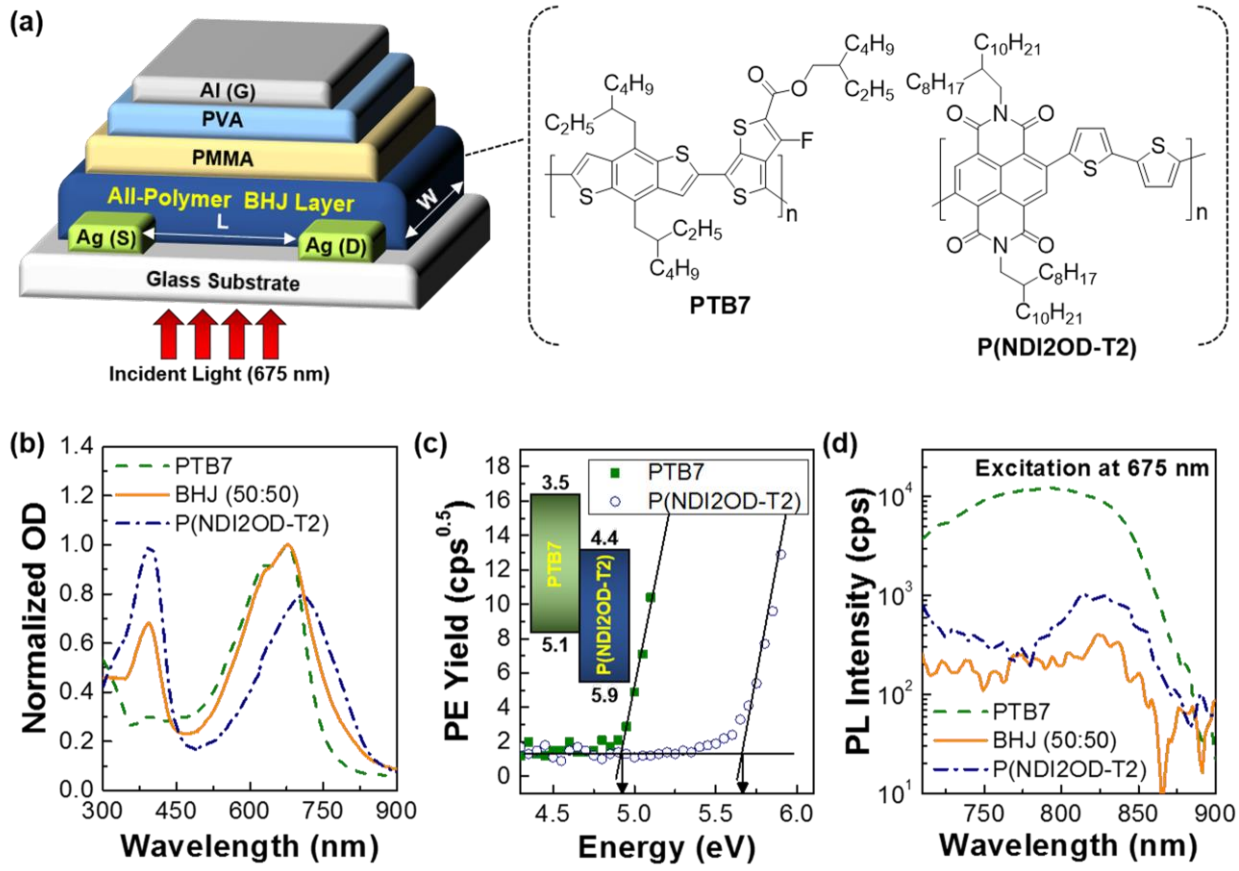

Figure 1. (a) Device structure of all-polymer phototransistor and chemical structures of PTB7 and P(NDI2OD-T2): L and W denote the channel length and width of the present device. (b) Optical absorption spectra of pristine and BHJ films. (c) Photoelectron (PE) yield spectra of pristine PTB7 and P(NDI2OD-T2) thin films. (d) Photoluminescence (PL) spectra of pristine and PTB7:P(NDI2OD-T2) BHJ films.

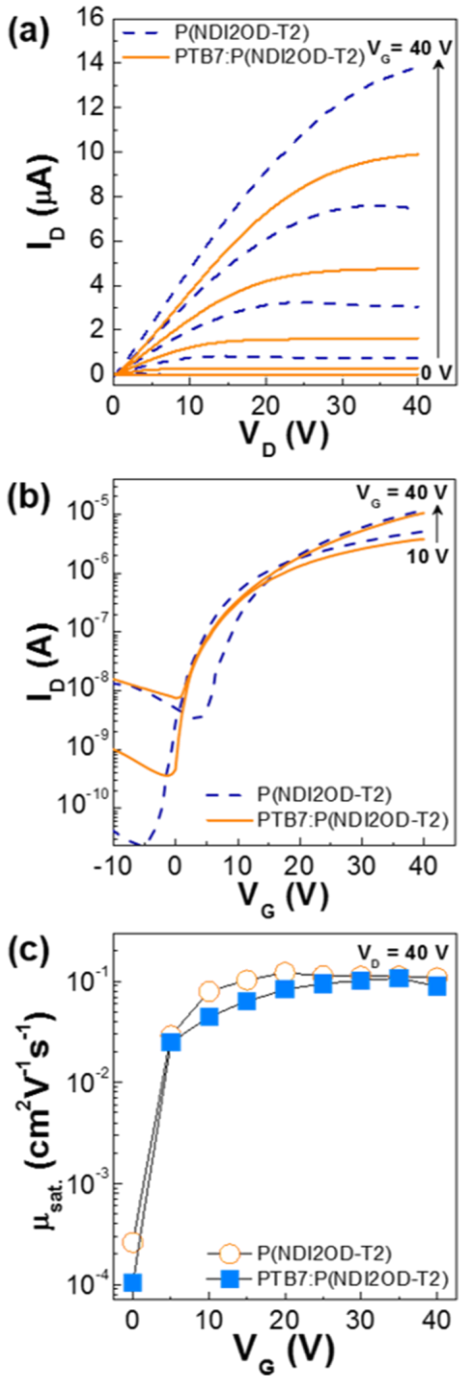

Figure 2. Output and transfer curves for (a) pristine P(NDI2OD-T2) and (b) PTB7:P(NDI2OD-T2) transistors in the dark. (c) Gate-voltage dependent mobility of pristine P(NDI2OD-T2) and PTB7:P(NDI2OD-T2) transistors.

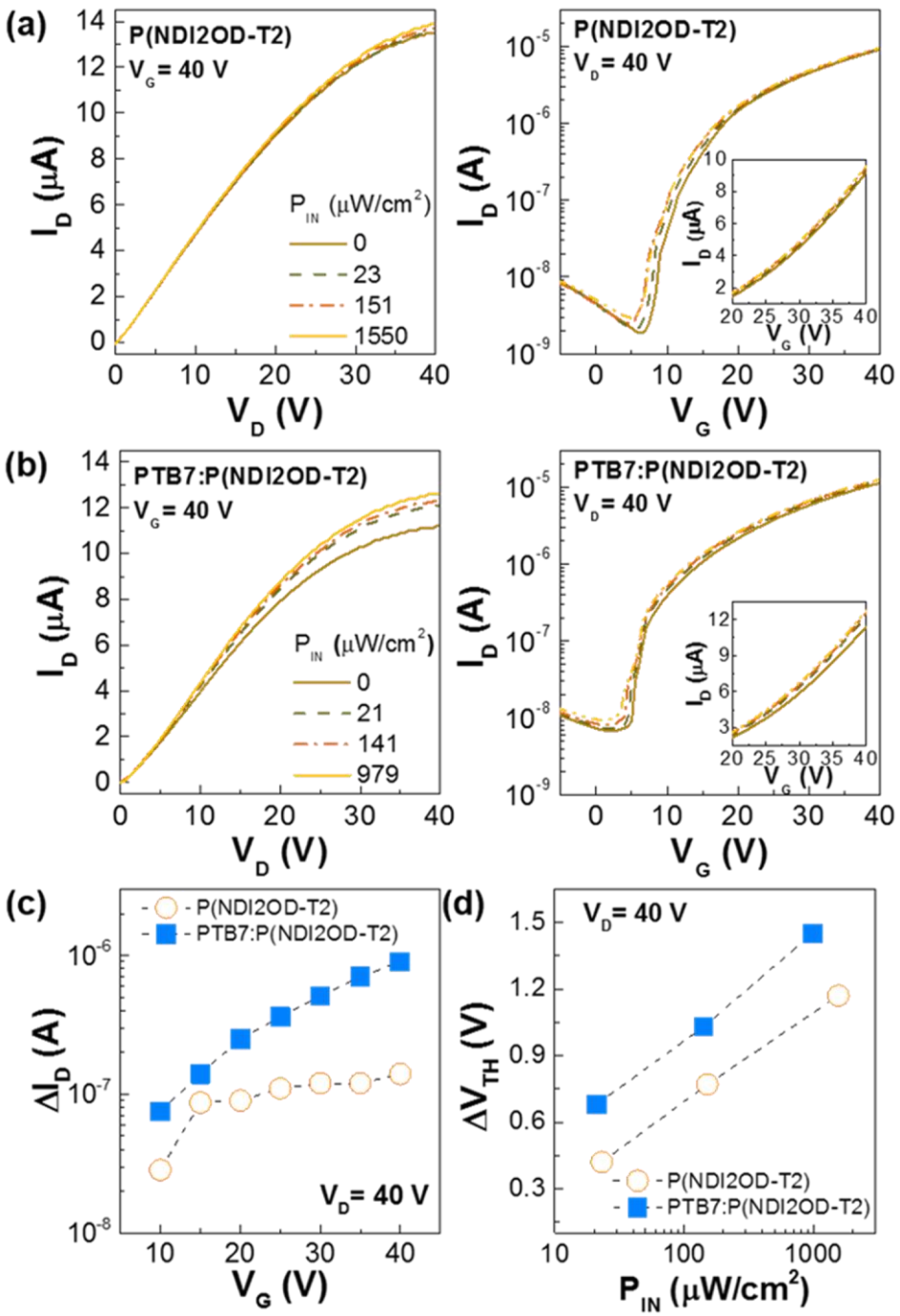

Figure 3. Output and transfer curves for (a) P(NDI2OD-T2)-only and (b) PTB7:P(NDI2OD-T2) phototransistors under illumination with 675 nm monochromatic light. (c) Change in the drain current (ΔI_D) as a function of gate voltage (V_G). (d) Change in the threshold voltage (ΔV_{TH}) as a function of light intensity (P_{IN}).

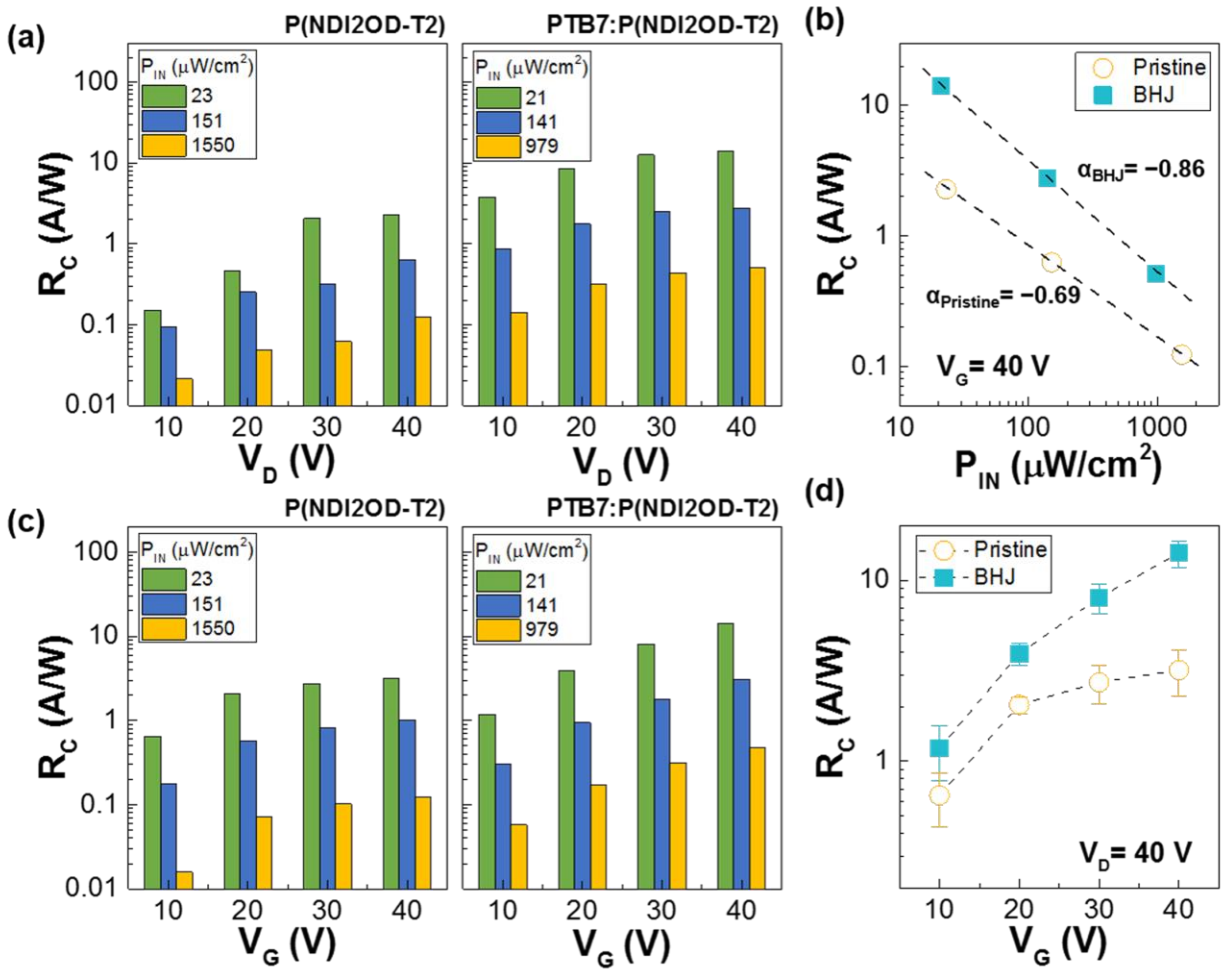

Figure 4. (a) Photoresponsivity as a function of drain voltage (V_D) for P(NDI2OD-T2)-only and PTB7:P(NDI2OD-T2) phototransistors at different levels of light intensity (P_{IN}). (b) Photoresponsivity as a function of light intensity (P_{IN}) for P(NDI2OD-T2)-only and PTB7:P(NDI2OD-T2) phototransistors. Note that the R_C values were obtained from the output curves in Figure 3a, which were measured at V_D and V_G = 40 V. (c) Photoresponsivity as a function of gate voltage (V_G) for P(NDI2OD-T2)-only and PTB7:P(NDI2OD-T2) phototransistors at different levels of light intensity (P_{IN}). (d) Photoresponsivity as a function of light intensity (P_{IN}) for P(NDI2OD-T2)-only and PTB7:P(NDI2OD-T2) phototransistors. Note that the R_C values were obtained from the transfer curves for more than five devices with two sub-cells per each device.

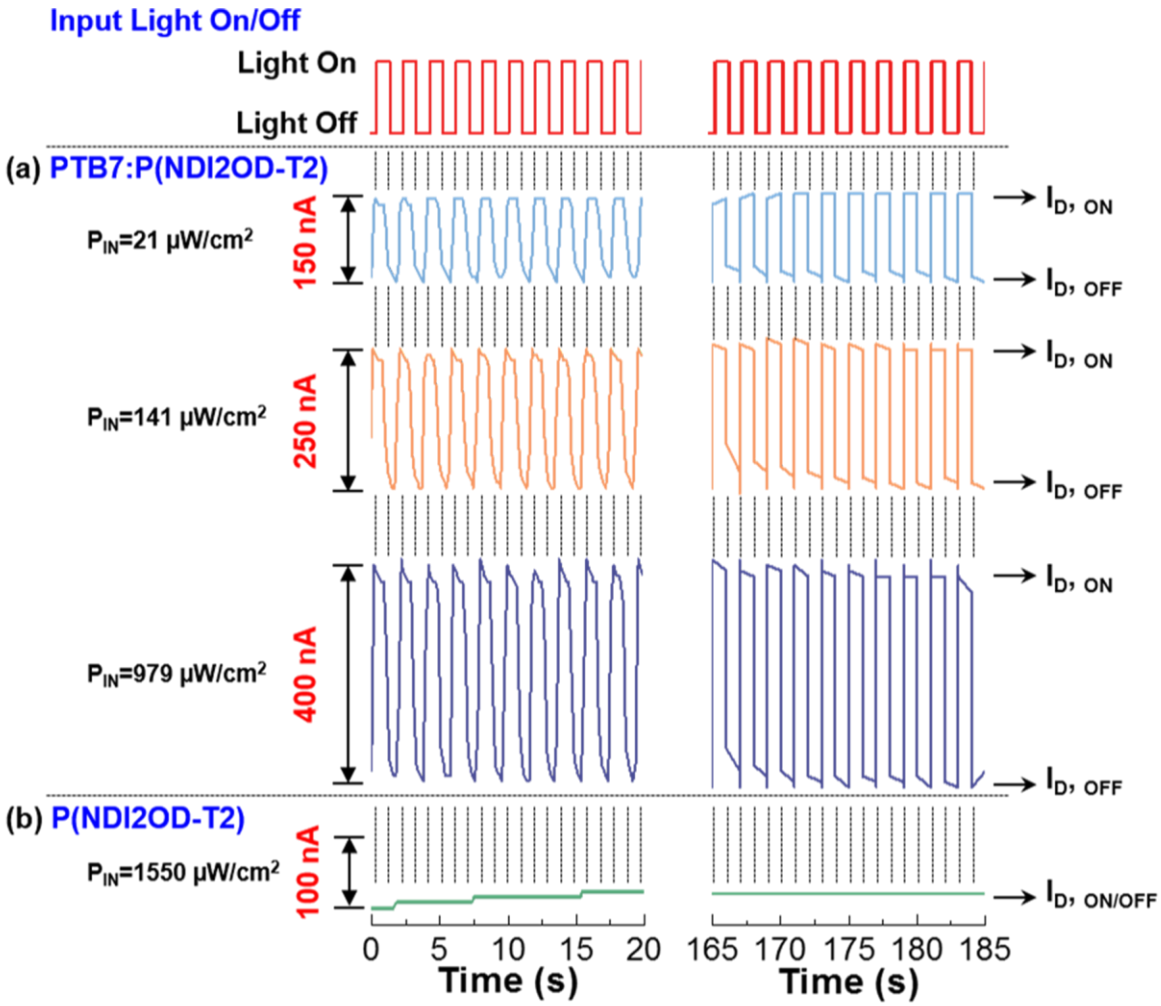

Figure 5. Photoresponses of devices (V_D = 20 V and V_G = 40 V) according to the on/off modulation of input light with a time interval of 1 s: (a) PTB7:P(NDI2OD-T2) and (b) P(NDI2OD-T2)-only phototransistors.

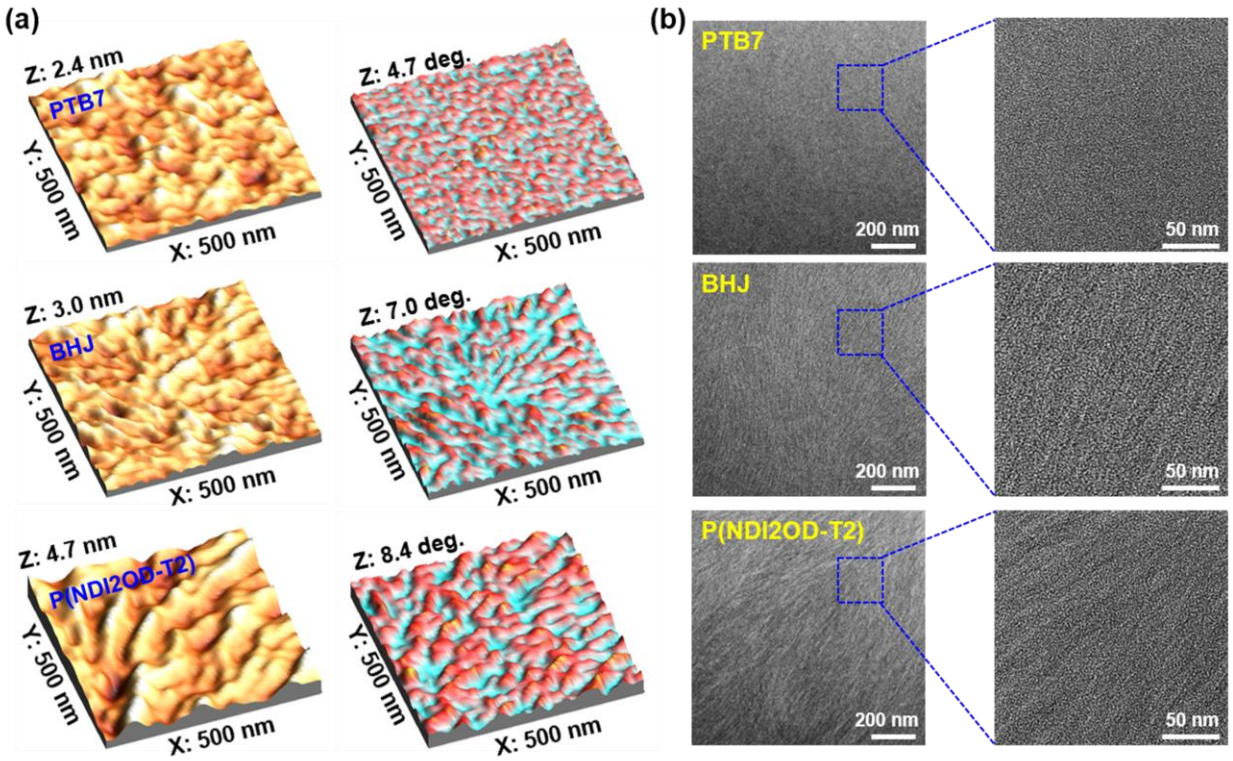

Figure 6. (a) 3D-height and phase mode AFM images, and (b) TEM images of pristine PTB7 (top), PTB7:P(NDI2OD-T2) BHJ (middle), and pristine P(NDI2OD-T2) (bottom) thin films coated on glass substrates.

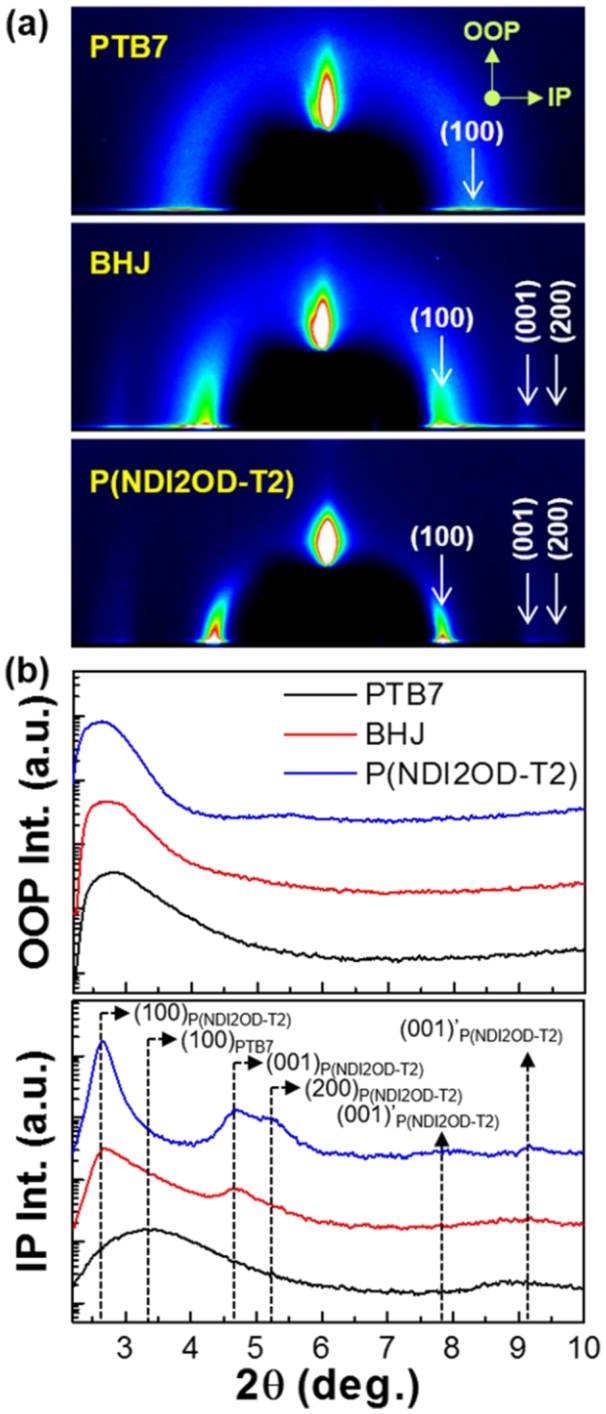

Figure 7. (a) 2D GIXD images and (b) 1D profiles in the OOP and IP directions for pristine PTB7, PTB7:P(NDI2OD-T2), and pristine P(NDI2OD-T2) thin films coated on glass substrates.

<TOC Graphic>

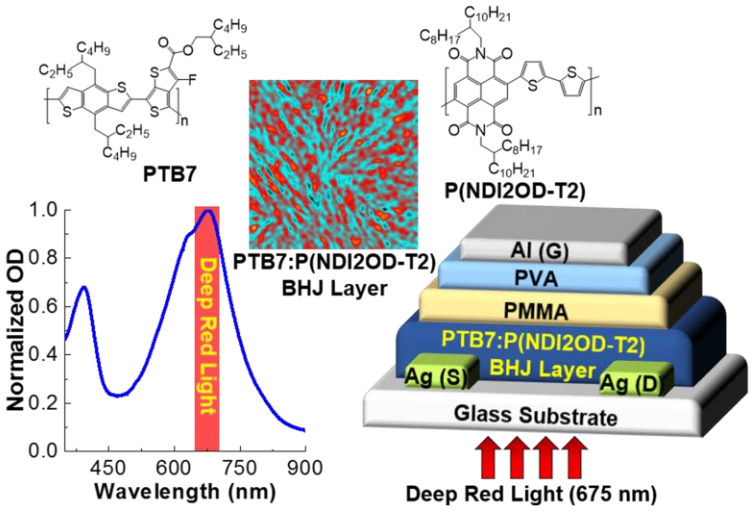
PTB7
P(NDI2OD-T2)
PTB7:P(NDI2OD-T2)
BHJ Layer
Normalized OD
Wavelength (nm)
Deep Red Light
Al (G)
PVA
PMMA
PTB7:P(NDI2OD-T2)
BHJ Layer
Ag (S)
Ag (D)
Glass Substrate
Deep Red Light (675 nm)